Journal of Materials Chemistry C

PAPER

View Article Online
View Journal | View Issue

Cite this: J. Mater. Chem. C, 2014, 2, 4879

Synthesis and characterization of benzo- and naphtho[2,1-*b*:3,4-*b*′]dithiophene-containing oligomers for photovoltaic applications†‡

Mirjam Löbert,[a] Amaresh Mishra,[a] Christian Uhrich,[b] Martin Pfeiffer[b] and Peter Bäuerle*[a]

Received 19th February 2014
Accepted 21st March 2014

DOI: 10.1039/c4tc00335g

www.rsc.org/MaterialsC

Dicyanovinyl (DCV) end-capped oligomers **1–7** containing fused benzo[2,1-*b*:3,4-*b*′]dithiophene (BDT) and naphtho[2,1-*b*:3,4-*b*′]dithiophene (NDT) as central cores have been synthesized and characterized. These oligomers show excellent thermal stability due to the insertion of the central fused ring system thus allowing purification by gradient sublimation in high yield. With respect to the reference compound, non-fused tetramer **DCV4T**, the new oligomers showed hypsochromic shifts in absorption and emission spectra and larger band gaps in thin films. Due to high lying LUMO energy levels, they exhibit sufficient energy offset with respect to C_{60} to allow for efficient charge transfer in organic solar cells. At the same time, low-lying HOMO energy levels result in high open-circuit voltages (V_{OC}). As a result, planar heterojunction (PHJ) solar cells derived from the novel oligomers and C_{60} provide very high open circuit voltages (V_{OC}) of up to 1.21 V and power conversion efficiencies (PCEs) of up to 2.7%. Bulk-heterojunction (BHJ) devices comprising oligomers **1–4** and C_{60} display a slightly lower V_{OC} of 1 V leading to efficiencies as high as 3.6%.

Introduction

Over the last few years, great progress has been made for organic solar cells (OSC) based on structurally defined π-conjugated oligomers, typically referred to as "small molecules", as electron donors and fullerene derivatives as electron acceptors.[1–3] The "driving force" for this rapid development comes from the versatile design of appropriate p-type semiconducting oligomers and optimization of device fabrication conditions in planar-heterojunction (PHJ) and bulk-heterojunction (BHJ) architectures. High power conversion efficiencies (PCEs) of 8–9% (ref. 4–6) and 10.1% (ref. 7) have very recently been achieved for solution-processed oligomer BHJ single junction cells and the first oligomer/oligomer tandem cell, respectively. Triple cells containing evaporated oligomers reached record efficiencies of 12.0% at the beginning of last year.[8] Structurally defined oligomers comprise several inherent advantages compared to conjugated polymers, such as involving straightforward synthesis and purification processes leading to well-defined molecular structures with defined molecular weight. Thus, they can be prepared with high purity and reproducibility.[9]

Further development of new π-conjugated molecules is therefore of considerable interest in order to provide specially tuned materials with appropriate physical properties. In this context, special attention has recently been paid on planar molecules comprising fused ring systems. Such molecules combine excellent charge carrier mobilities in organic field-effect transistors (OFET) and high thermal stability at the same time.[10–12] Among them, benzo[2,1-*b*:3,4-*b*′]dithiophene (BDT) and naphtho[2,1-*b*:3,4-*b*′]dithiophene (NDT) represent promising fused thiophene-based systems, which were included in various copolymers and tested as donor materials in OSCs.[13–19] It has been shown that in these systems annulation lowers the HOMO energy level of the polymer, thus an improvement of air stability and higher open circuit voltages (V_{OC}) in OSCs were shown. Müllen *et al.* recently reported that BDT-containing polythiophenes had low-lying HOMO energy levels and favorable aggregation behavior resulting in higher field-effect mobilities in comparison to the polythiophene counterpart.[20,21] OSCs of the BDT-polymer in combination with soluble fullerene derivative $PC_{71}BM$ as the acceptor gave a PCE of 2.7%.[13]

To date, only one example of a BDT-containing π-conjugated oligomer is reported. In comparison to the corresponding bithiophene analogue introduction of fused rings resulted in a hypsochromic shift of the longest wavelength absorption and a lowering of the HOMO energy level which was attributed to the reduction of the effective conjugation length because of the

[a]Institute of Organic Chemistry II and Advanced Materials, University of Ulm, Albert-Einstein-Allee 11, D-89081 Ulm, Germany. E-mail: peter.baeuerle@uni-ulm.de
[b]Heliatek GmbH, Treidlerstr. 3, 01139 Dresden, Germany

† In memoriam Michael Bendikov.

‡ Electronic supplementary information (ESI) available. See DOI: 10.1039/c4tc00335g

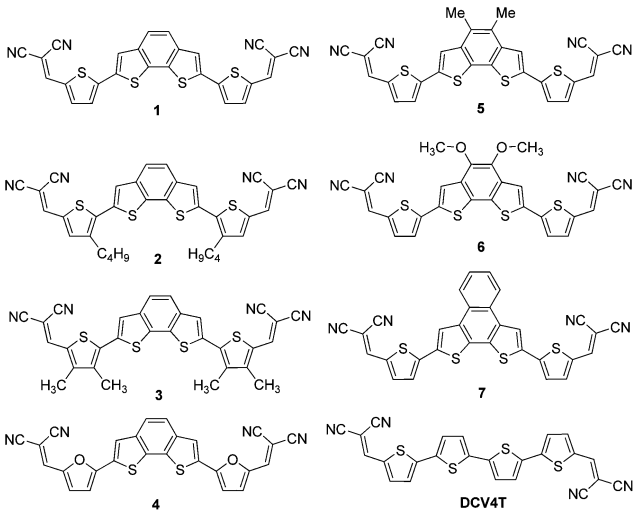

Chart 1 Series of benzo[2,1-*b*:3,4-*b*′]dithiophene-based oligomers **1–6** and naphtho[2,1-*b*:3,4-*b*′]dithiophene-based oligomer **7**. The molecular structure of **DCV4T** is shown for comparison.

bent structure of the BDT unit.[22] Herein, we now present a series of tetramers incorporating the BDT and NDT unit as a core motif. We further studied the influence of the molecular rigidity on optoelectronic properties and energy levels of the frontier orbitals and compared the data to quaterthiophene derivative **DCV4T** as a reference which was reported previously[23] (Chart 1). Additionally, the influence of different side chains and the replacement of the terminal thiophenes by furans were investigated. Finally, a correlation of the structural features and resulting properties with the solar cell performance was set up in order to gain further insight into molecular structure–device performance relationships.

Results and discussion

Synthesis of BDT-based and NDT-based oligomers

Benzodithiophene containing oligomers **1–4** were synthesized in 81% to 90% yield by Pd^0-catalyzed Stille-type cross-coupling of DCV-capped terminal building blocks **10**,[24] **12**, **13**,[25] **15**, and distannylated benzodithiophene BDT **9** (Scheme 1). 2-[(5-Bromo-4-butylthien-2-yl)methylene]malononitrile **12** was synthesized in 90% yield by a Knoevenagel condensation of 5-bromo-4-butylthiophene-2-carbaldehyde **11** (ref. 26) and malononitrile in the presence of β-alanine as the catalyst. 2-[(5-Bromofur-2-yl)methylene]malononitrile **15** was synthesized in 65% yield by a Knoevenagel reaction of 5-bromofuran-2-carbaldehyde **14** and malononitrile using a catalytic amount of piperidine as a base. Distannylation of BDT **8** (ref. 27) was carried out by lithiation using *n*-butyl lithium and subsequent quenching with trimethyltin chloride in 94% yield.

Oligomers **5–7** were synthesized by Pd^0-catalyzed Stille-type cross-coupling reaction of bromo-derivative **10** with distannylated central units **22**, **26**, and **30** in yield between 83% and 96%. Synthesis of stannyl derivative **22** (Scheme 2) started with 3,3′-dibromo-5,5′-bistrimethylsilyl-2,2′-bithiophene **19**, which

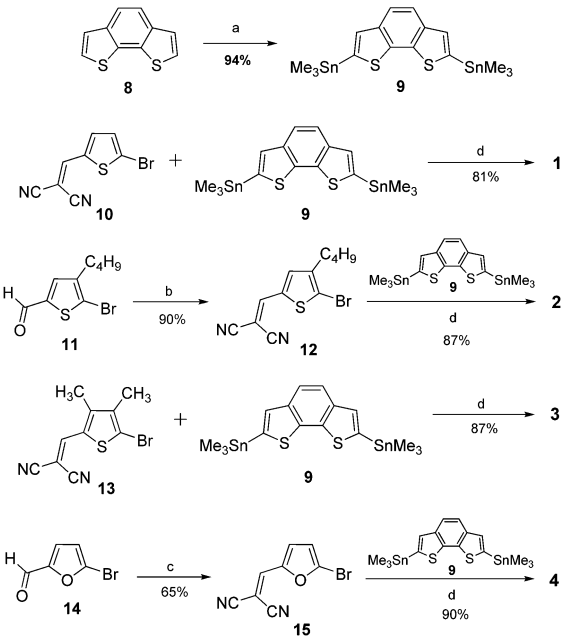

Scheme 1 Synthesis of benzodithiophene containing oligomers **1–4**. (a) (1) *n*-BuLi, THF, −78 °C, 1 h; (2) rt, 2 h; (3) Me_3SnCl, THF, −78 °C, 1 h; (b) malononitrile, β-alanine, ethanol, reflux, 15 h; (c) malononitrile, piperidine, DCE, reflux, 20 h; (d) $Pd(PPh_3)_4$, DMF, 80 °C, 15 h.

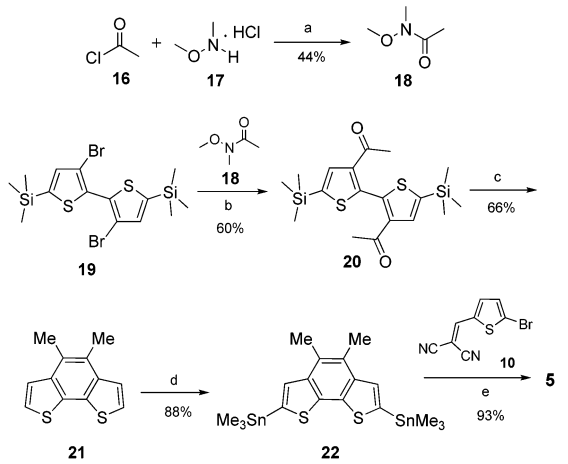

Scheme 2 Synthesis of benzodithiophene-containing oligomer **5**. (a) (1) Triethylamine, DCM, 1 h, 0 °C; (2) 2 h, rt; (b) (1) *n*-BuLi, THF, −78 °C, 30 min; (2) **18**, 45 min, −78 °C; (c) (1) $TiCl_4$, Zn, THF, 2 h, 0 °C; (2) **20**, THF, 15 h, Δ; (3) THF, TBAF, 15 min, rt; (d) (1) *n*-BuLi, THF, −78 °C, 30 min; (2) Me_3SnCl, 2 h, −78 °C; (e) $Pd(PPh_3)_4$, DMF, 80 °C, 15 h.

was synthesized as described in the literature.[28] Firstly, diacetyl **20** was synthesized in 60% yield by lithiation of bithiophene **19** using *n*-BuLi followed by quenching with *N*-methoxy-*N*-methylacetamide[29] **18**. The second step was an intramolecular McMurry reaction using $TiCl_4$ and elementary zinc followed by deprotection of the trimethylsilyl (TMS) groups using tetra-*n*-butylammonium fluoride trihydrate (TBAF) to afford 4,5-dimethylbenzo[2,1-*b*:3,4-*b*′]dithiophene **21** in a yield of 66% (for two

steps). Finally, bithiophene **21** was reacted with *n*-BuLi and trimethyltin chloride to give stannyl derivative **22** in 88% yield.

Benzo[2,1-*b*:3,4-*b*′]dithiophene-4,5-dione **23** was readily synthesized as described in the literature.[30] In the first step, twofold esterification of **23** to acetylated derivative **24** was achieved in 67% yield by reaction with acetic anhydride, zinc, and triethylamine. This reaction was carried out according to the synthesis of benzo[1,2-*b*:4,3-*b*′]dithiophene-4,5-diyldiacetate as described in the literature.[31] Then, a twofold etherification with cesium carbonate and methyl iodide afforded dimethoxy-BDT **25** in 86% yield. Stannylation of **25** with *n*-BuLi and trimethyltin chloride gave bis-stannylated **26** in 90% yield (Scheme 3).

Synthesis of naphtho[2,1-*b*:3,4-*b*′]bithiophene and its derivatives is described in the literature. The fused ring system was on one hand synthesized *via* a palladium-catalyzed coupling of 3,3′-diiodo-2,2′-bithiophene and an alkyne[14] or *via* oxidative cyclization on the other hand.[32,33] We developed a new synthesis route, which includes a twofold Stille cross-coupling reaction of [3,3'-bis(trimethylstannyl)-2,2'-bithien-5,5'-diyl]-bis(trimethylsilane) and 1,2-dibromobenzene **28** (Scheme 4). Stannyl derivative **27** was obtained in a yield of 88% by quenching the lithiated species of bithiophene **19** with trimethyltin chloride. The Stille reaction of **27** with 1,2-dibromobenzene **28** and *in situ* deprotection of the trimethylsilyl groups gave **29** in 53% yield (for two steps) which was stannylated using *n*-BuLi and trimethylstannyl chloride to obtain NDT-derivative **30** in a yield of 94%.

Thermal properties

Thermal stability of optoelectronic materials is of paramount importance for the construction of organic solar cells when prepared by vacuum-deposition techniques at higher temperatures. Therefore, we investigated melting points and decomposition temperatures of the BDT- and NDT-based target molecules **1–7** by differential scanning calorimetry (DSC) and thermo-gravimetric analysis (TGA) under an inert atmosphere at a heating rate of 10 °C min^{-1} (Fig. 1, Table 1). BDTs **1–6** melted between 311 °C and 458 °C and do not decompose below 380 °C. NDT **7** showed an even higher melting temperature of 473 °C with a decomposition temperature of 480 °C. The excellent thermal stability of oligomers **1–7** was confirmed by TGA measurements, also showing decomposition temperatures (T_d) with 5% weight loss above 380 °C.

The melting temperature (T_m) of oligomer **1** is 30 °C higher than that of **DCV4T** pointing to stronger intermolecular interactions due to the planarization of the BDT unit. The furan

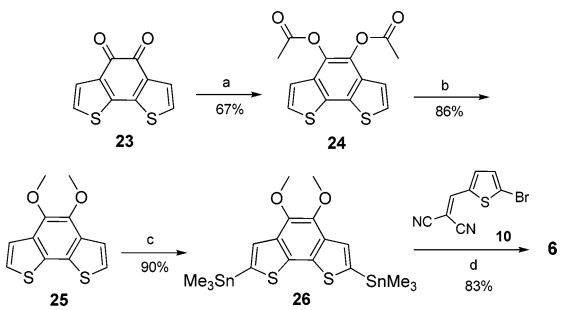

Scheme 3 Synthesis of 4,5-dimethoxybenzo[2,1-*b*:3,4-*b*′]dithiophene containing oligomer **6**. (a) Zn, triethylamine, DCM, acetic anhydride, 15 h, rt; (b) Cs_2CO_3, MeI, acetonitrile, 80 °C, 72 h; (c) (1) *n*-BuLi, THF, −78 °C, 30 min; (2) Me_3SnCl, 2 h, −78 °C, 12 h, rt; (d) $Pd(PPh_3)_4$, DMF, 80 °C, 15 h.

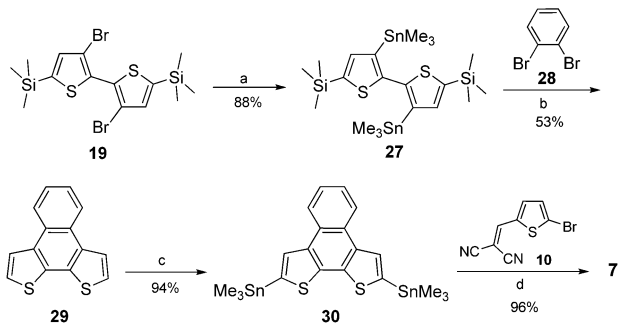

Scheme 4 Synthesis of naphtho[2,1-*b*:3,4-*b*′]bithiophene-containing oligomer **7**. (a) (1) *n*-BuLi, THF, −78 °C, 30 min; (2) Me_3SnCl, 2 h, −78 °C, 2 h, rt; (b) (1) $Pd_2(dba)_3 \cdot CHCl_3$, $HP(^tBu)_3BF_4$, DMF, 100 °C, 2 days; (2) TBAF, THF, 15 min, rt; (c) (1) *n*-BuLi, THF, −78 °C, 30 min; (2) Me_3SnCl, 2 h, −78 °C; (d) $Pd(PPh_3)_4$, DMF, 80 °C, 15 h.

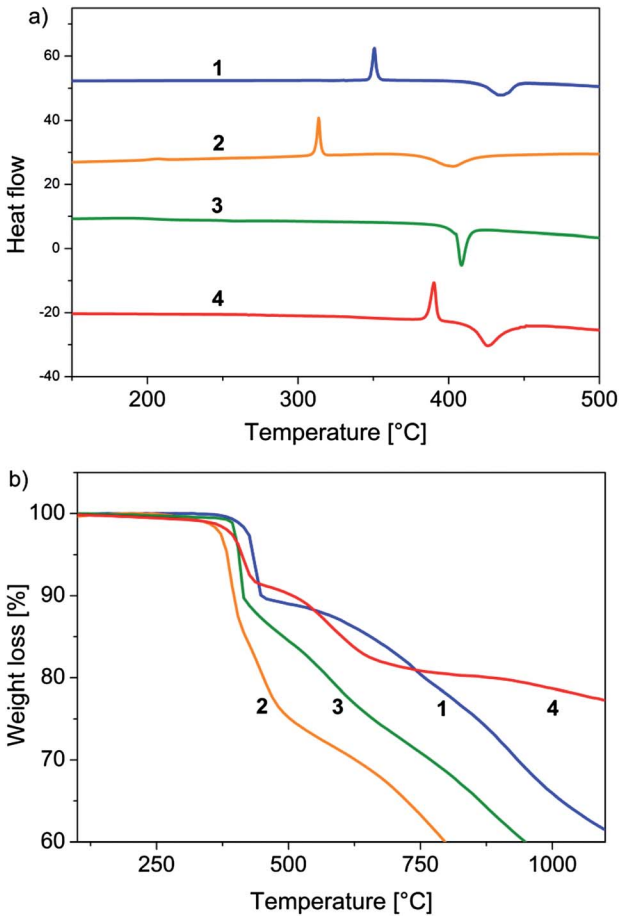

Fig. 1 (a) DSC curves for benzodithiophenes **1–4** measured under argon flow at a heating rate of 10 °C min^{-1}. (b) TGA curves for **1–4** measured under nitrogen flow at a heating rate of 10 °C min^{-1}.

Table 1 Thermal properties of oligomers **1–7** and **DCV4T**

Oligomer	T_m[a]	T_d[a]	T_d[b]
DCV4T	320	424	411
1	350	431	430
2	311	383	382
3	—	407	405
4	386	411	412
5	458	463	440
6	404	410	400
7	473	480	472

[a] Melting temperature (T_m) and decomposition temperature (T_d) determined from DSC. [b] Decomposition temperature corresponding to 5% weight loss in N_2 determined by TGA.

containing oligomer **4** showed a 36 °C higher melting point further supporting the higher intermolecular interactions of furan-containing oligomers compared to oligothiophenes.[34] Butyl side chains decreased the melting temperature and compound **2** melted at 311 °C which is 39 °C lower than that of BDT **1**. Oligomer **3** did not show any phase transition before decomposition. The substituents at the ethylene bridge of the BDT unit of oligomers **5–7** resulted in an increase of the melting temperature (Fig. S1†). BDT **5–7** showed a strong exothermic peak immediately after melting. The planar NDT containing oligomer **7** showed the highest melting temperature of 473 °C. The compounds were purified by gradient vacuum sublimation.

Optical spectroscopy

The optical properties of the BDT-based oligomers **1–7** were determined by UV-vis and fluorescence spectroscopy in dichloromethane and in thin films prepared by vacuum sublimation. All data are summarized in Table 2. Representative solution and thin film spectra are shown in Fig. 2 and S2.†

In solution, BDT containing oligomers **1–6** showed an absorption maximum between 484 nm and 497 nm. Each corresponds to the π–π* (HOMO–LUMO) transition of the conjugated π-system. The absorption bands of oligomers **1–6** are hypsochromically shifted compared to **DCV4T** due to lowering of the HOMO energy level as a consequence of the fused BDT unit. In contrast to **DCV4T**, BDT-oligomer **1** showed a strong alternation of the absorption band with two distinct vibronic transitions appearing at 489 nm and 506 nm. The emission maximum of **1** is about 42 nm blue-shifted in comparison to **DCV4T** showing its maximum at 565 nm. Similar vibronic splitting of the absorption and emission bands was also observed for the furan-containing oligomer **4**. The smaller Stokes shift for **4** compared to **1** can be assigned to the higher

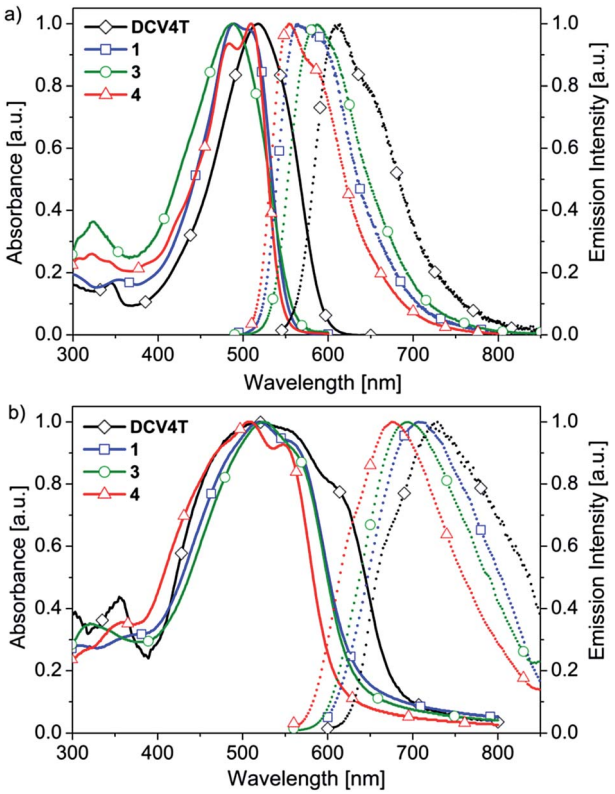

Fig. 2 (a) Representative absorption and fluorescence spectra of benzodithiophene **1**, **3**, and **4** in dichloromethane at room temperature. (b) Thin film (30 nm) absorbance and fluorescence spectra of benzodithiophene **1**, **3**, and **4**. Thin films were prepared by vacuum sublimation. The absorption and emission spectra of **DCV4T** are included for comparison.

Table 2 Optical data of molecules **1–7** compared to **DCV4T**. The values in brackets represent shoulders

	Solution					Film		
Compound	λ_{abs} [nm]	ε_{max} [L mol^{-1} cm^{-1}]	Stokes shift [cm^{-1}]	λ_{em} [nm]	ΔE_{opt}[a] [eV]	λ_{abs} [nm]	λ_{em} [nm]	ΔE_{opt}[b] [eV]
DCV4T (ref. 21)	518	66 800	2922	612 (651)	2.09	560	670	1.78
1	489 (506)	74 500	1856	565 (588)	2.23	518	707	1.95
2	485	54 100	3612	588	2.20	529	715	1.94
3	487	—	3381	587	2.17	522	694	1.96
4	484, 509	—	1628	555 (582)	2.26	505	675	2.03
5	494	—	3982	615 (650)	2.19	531	735	1.87
6	497 (516)	—	2373	588	2.20	528	725	1.90
7	512 (537)	—	2093	605 (648)	2.12	549	766	1.80

[a] Estimated using the onset of the UV-Vis spectra in DCM. [b] Estimated using the onset of the UV-Vis spectra of films prepared by vacuum sublimation.

rigidity of the oligofurans in comparison to that of oligothiophenes.[34]

The absorption and fluorescence spectra of butyl- and methyl-substituted oligomers **2** and **3** displayed structureless bands due to the presence of alkyl side chains. The Stokes shift of these two oligomers is larger compared to that of **1**, **4**, and **DCV4T**, which is an indication for a higher twist between the alkylated thiophenes and the BDT unit.

In comparison to oligomer **1**, the insertion of electron donating methyl and methoxy groups at the BDT units in **5** and **6** showed only a small influence on the absorption behaviour. On the other hand, the emission maxima of oligomers **5** and **6** are 50 nm and 23 nm red-shifted compared to **1** resulting in a larger Stokes shift of 3982 cm^{-1} and 2373 cm^{-1}, respectively. The larger Stokes shift further confirms the steric hinderance in oligomers **5** and **6** indicating a significant structural reorganization on photoexcitation.

The molar extinction coefficient of **1** was about 7700 L mol^{-1} cm^{-1} higher than that of the parent **DCV4T**, while due to molecular flexibility the molar extinction coefficient is reduced for oligomer **2**. The molar extinction coefficient of oligomers **3**–**7** could not be determined due to their poor solubility.

NDT-containing oligomer **7** showed a bathochromic shift of the absorption band in comparison to BDT **1**–**6** due to the higher electron-donating strength of the NDT unit. The absorption maximum of **7** was located at 512 nm with a shoulder at around 537 nm. The emission maximum of **7** was strongly red-shifted by $\Delta\lambda = 40$ nm compared to **1** resulting in a slightly larger Stoke shift of 2093 cm^{-1}.

In solution the optical energy gap of oligomers **1**–**6** is found to be slightly larger (2.17–2.26 eV) compared to 2.09 eV for **DCV4T**. While, NDT **7** showed a very similar energy gap of 2.12 eV compared to **DCV4T**.

Thin film absorption and emission spectra of BDTs **1**–**7** are significantly broadened and bathochromically shifted compared to the solution spectra (Fig. 2 and S2†). This red-shift and spectral broadening in thin films suggest higher planarity of the molecules in films which induces a higher ordering and an increase of the intermolecular interactions. The absorption maxima of BDT oligomers **1**–**6** are localized between 505 nm and 529 nm and the emission maxima between 675 nm and 735 nm. The absorption maximum of NDT **7** is further red-shifted to 549 nm and the emission maximum to 766 nm. The optical band gaps in thin films are lowered by about 0.3 eV compared to the gaps obtained from solution spectra.

Cyclic voltammetry

The redox properties of oligomers **1**–**4** have been measured in 0.1 M tetrachloroethane–$TBAPF_6$ at 80 °C. All data are summarized in Table 3 and the DPV of oligomer **1** is shown as an example in Fig. 3. Oligomer **1** showed two reversible one-electron oxidation waves at 0.99 V and 1.33 V indicating the formation of stable radical cations and dications, respectively. One quasi-reversible reduction wave was observed at −1.41 V which is assigned to the reduction of the DCV end groups. As a consequence of the fused BDT unit, the oxidation potentials of oligomer **1** are shifted to slightly higher potentials ($\Delta E_{ox} = 0.15$ V and 0.13 V) compared to **DCV4T** whereas no change was observed for the reduction potential. The oxidation potentials of oligomer **2** are very similar to that of **1**. Oligomer **3** containing four methyl groups showed slightly lower oxidation potentials ($\Delta E_{ox} = 0.05$ V and ~0.14 V) compared to **1** and **2**. In contrast, furan-containing oligomer **4** did not show a reversible oxidation behavior and the waves were shifted to lower potentials of 0.85 V and 1.17 V. Similar behavior is also reported for oligofurans.[34]

The HOMO and LUMO energy levels of oligomers **1**–**4** were calculated from the onset values of the first oxidation and reduction wave using the standard approximation that the Fc/Fc^+ HOMO energy level is −5.1 eV *versus* vacuum.[35] The results are presented in Fig. 4 and the data are compiled in Table 3. The HOMO and LUMO levels of compounds **1** and **2** are identical showing an electrochemical band gap of 2.19 eV. The LUMO energy level of oligomer **3** is similar to **1** and **2** but showed a

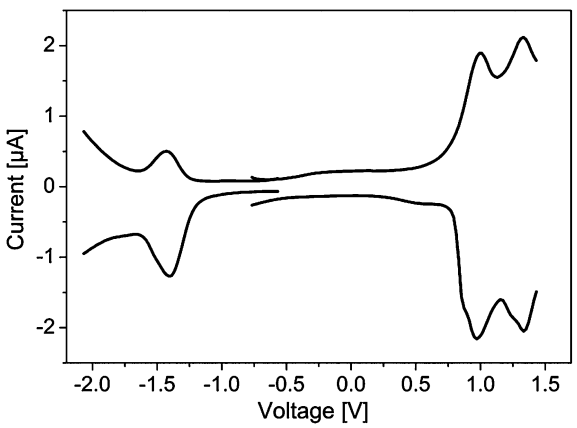

Fig. 3 Representative DPV of benzodithiophene-containing oligomer **1** measured in TCE–$TBAPF_6$ (0.1 M), $c \approx 1 \times 10^{-3}$ mol L^{-1}, 80 °C, scan rate = 100 mV s^{-1}.

Table 3 Electrochemical data of benzodithiophene-containing oligomers **1**–**4** compared to **DCV4T**[a]

Compound	E_{ox1} [V]	E_{ox2} [V]	E_{red} [V]	HOMO[b] [eV]	LUMO[b] [eV]	ΔE_{CV}[c]
DCV4T (ref. 21)	0.84	1.20	−1.41	−5.85	−3.87	1.98
1	0.99	1.33	−1.41	−6.00	−3.81	2.19
2	1.00	1.30	−1.47	−5.98	−3.80	2.18
3	0.94	1.19	−1.48	−5.89	−3.80	2.09
4	0.85	1.17	−1.57	−5.81	−3.62	2.19

[a] Measured in TCE–$TBAPF_6$ (0.1 M), [compound] = 10^{-3} mol L^{-1}, 80 °C, $V = 100$ mV s^{-1}, *vs.* Fc^+/Fc. [b] Calculated from the onset of the first oxidation and reduction wave, set Fc^+/Fc $E_{HOMO} = -5.1$ eV. [c] Calculated from the difference between the values of $E_{onset,red1}$ and $E_{onset,ox1}$.

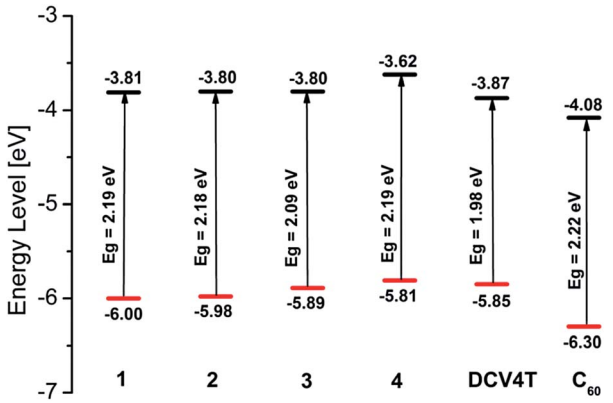

Fig. 4 Representation of HOMO/LUMO energies of oligomers **1–4** and **DCV4T** derived from electrochemical data compared to C_{60}. The HOMO/LUMO energy levels of C_{60} are taken from the literature[36] and were determined from the onset of the first oxidation and reduction waves measured in 0.1 M $TBAPF_6$–tetrachloroethane.

slightly higher HOMO level, which, resulted in a lower electrochemical band gap of 2.09 eV. Compound **4** comprising furan units showed HOMO and LUMO energy values which are about 0.2 eV higher than that of **1**, thus an identical electrochemical band gap of 2.19 eV. The redox properties of oligomers **5–7** could not be determined due to their low solubility. As can be seen in Fig. 5 the low lying HOMO energy levels of these oligomers could be favorable for obtaining higher V_{OC} in organic solar cells using C_{60} as an acceptor. It is known that the V_{OC} depends on the difference between the HOMO energy level of the donor and the LUMO energy level of the acceptor.

Preparation and characterization of vacuum-processed solar cells

The DCV end-capped oligomers **1–4** were tested as electron donor materials in PHJ and BHJ solar cells using fullerene C_{60} as an electron acceptor. The cells were prepared by vacuum sublimation following the m-i-p concept reported in the literature.[37,38]

Planar heterojunction solar cells

Planar heterojunction (PHJ) solar cells consist of a well-defined planar interface between the donor and the acceptor layer.

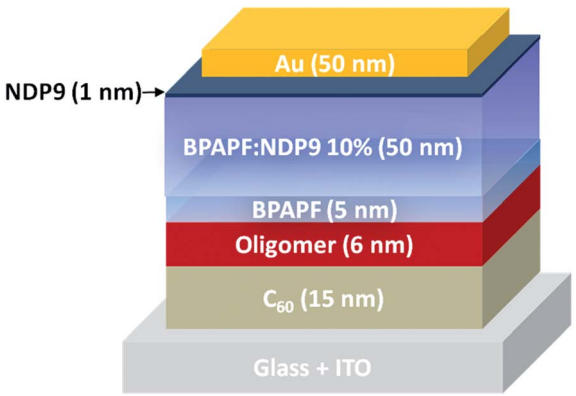

Fig. 5 General device architecture of investigated PHJ solar cells.

Consequently, the efficiency is not limited by charge carrier transport, but rather by the exciton diffusion length. The stack of the PHJ solar cells consisted of 15 nm C_{60} evaporated on an ITO-coated glass substrate, followed by deposition of a 6 nm donor layer of the respective oligomers **1–4**, 5 nm of undoped and 50 nm of p-doped 9,9-bis{4-[di-(*p*-biphenyl)aminophenyl]} fluorene (BPAPF) as a hole transport layer (HTL). The undoped BPAPF layer was introduced to avoid direct contact between the active layer and the p-doped BPAPF layer which otherwise could lead to quenching of excitons by the dopants.[39] As a p-dopant, NDP9 (10 wt%) was used. Another 1 nm thick layer of NDP9 was introduced between the HTL and the Au top contact to facilitate charge extraction (Fig. 5).

The PHJ solar cell parameters are summarized in Table 4. The current density–voltage (*J–V*) curves and the external quantum efficiency (EQE) spectra of the PHJ-devices are shown in Fig. 6. Oligomer **1** gave a PCE of 2.3%, with a short circuit current density (J_{SC}) of 4.7 mA cm^{-2}, a V_{OC} of 1.09 V, and a FF of 44%. The HOMO energy levels of oligomers **1–3** are reduced by 0.04 to 0.15 eV compared to **DCV4T**. In PHJ cells, V_{OC} scales linearly with the energy difference of the LUMO of the acceptor (C_{60}) and the HOMO of the donor.[40] Consequently, a very high V_{OC} of up to 1.21 V was obtained for oligomer **2**, which is one of the highest values ever reported for PHJ devices.[41,42] The higher V_{OC} value of **2** was consistent with its deeper low-lying HOMO energy level. On the other hand, the *J–V*-characteristics of the **2**-based device generated an s-kink due to an energetic barrier at the interface to the HTL resulting in a low FF of 37% and an efficiency of 1.5%. Even though, the HOMO energy level of oligomer **1** is the lowest among all oligomers, it yields only a V_{OC} of 1.09 V. This could be explained by the formation of pinholes in 6 nm thin films of the oligomer leading to some close contact between the C_{60} acceptor and BPAPF hole transporter, thus, making a direct contact between the cathode and anode. Friend and co-workers reported that these direct paths act as a shunt resistance in parallel with the active layer of the device, resulting in the lowering of V_{OC}.[43] Oligomers **3** and **4** showed V_{OC} values of 1.07 V and 0.97 V which correspond well to the energetic shift of the HOMO energy level with respect to the C_{60} acceptor. Furthermore, oligomers **3** and **4** based devices reached FF values of 44% and 59%, J_{SC}s of 4.3 mA cm^{-2} and 3.4 mA cm^{-2} and PCEs of 2.0 and 1.9%, respectively. The EQE spectrum of **4** is significantly shifted to lower wavelengths corroborated well with the thin film absorption spectrum (Fig. 6b).

PHJ solar cells prepared with oligomers **5** and **6** containing methyl and methoxy-substituents at the BDT unit achieved PCEs of 1.5% and 2.7%, respectively (Fig. S3†). The lower performance of **5** compared to **1** is due to the reduction in J_{SC}, V_{OC}, and FF values. However, the efficiency of oligomer **6** is very promising. In comparison to oligomer **1**, higher J_{SC} and V_{OC} values of 5.2 mA cm^{-2} and 1.15 V have been measured.

The perpendicular extension of the ring fusion in NDT-containing oligomer **7** led to a higher FF of 49% compared to 44% for BDT **1**. The *J–V* characteristics of NDT **7** showed a poor rectifying behavior in the dark, which is a hint for a poor film quality. A significantly lower V_{OC} of 0.90 V was measured for

Table 4 Photovoltaic parameters of planar heterojunction solar cells containing DCV end-capped BDT-containing oligomers **1–6** and NDT-derivative **7** compared to **DCV4T**. The active layer thickness is 6 nm

Compound	J_{SC}[a] [mA cm^{-2}]	V_{OC} [V]	FF [%]	η [%]	Saturation[b]	Intensity [mW cm^{-2}]
DCV4T	6.2	1.00	48	3.0	1.2	92
1	4.7	1.09	44	2.3	1.3	106
2	3.4	1.21	37	1.5	1.3	106
3	4.3	1.07	44	2.0	1.2	103
4	3.4	0.97	59	1.9	1.2	107
5	3.8	1.00	39	1.5	1.4	93
6	5.2	1.15	45	2.7	1.2	92
7	4.0	0.90	48	1.8	1.4	92

[a] Measured with mask and corrected to 100 mW cm^{-2}. [b] Defined as $J(-1\ V)/J_{SC}$.

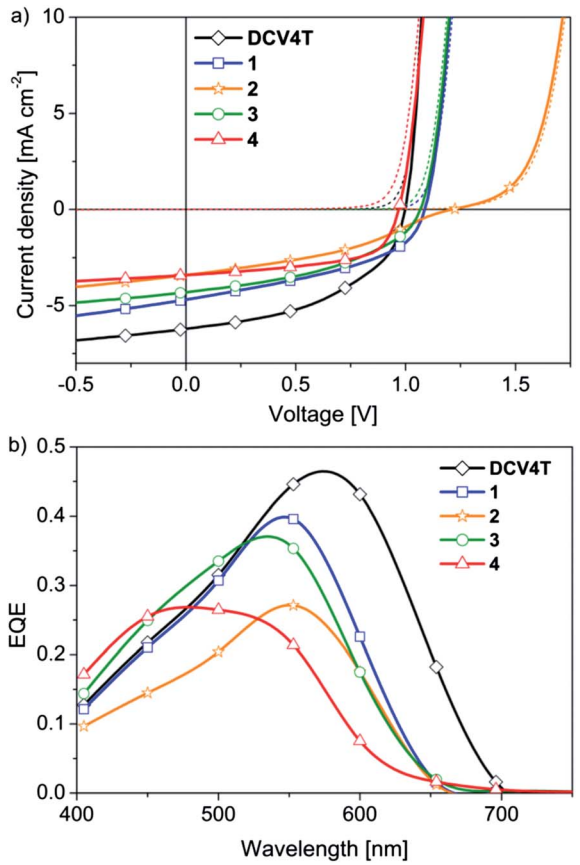

Fig. 6 (a) *J–V*-characteristics of planar heterojunction solar cells with DCV end-capped oligomers **1–4** and **DCV4T** as the donor material and C_{60} as an acceptor. (b) Corresponding EQE spectra of PHJ solar cells.

NDT **7**. This could be explained by a poor packing of NDT **7** in thin layers resulting in pinholes, which could lead to some close contact between the C_{60} and BPAPF hole transporter and thus reduces the V_{OC}. Together with a J_{SC} of 4.0 mA cm^{-2} the device generated a PCE of 1.8%.

In PHJ devices, reference compound **DCV4T** displayed the highest performance among all oligomers. Oligomers **1–7** exhibited significantly lower J_{SC} compared to **DCV4T** which was also reflected in their EQE spectra. The **DCV4T** device generated a PCE of 3.0% with a V_{OC} of 1.0 V and a higher J_{SC} of 6.2 mA cm^{-2} and a FF of 48%. The saturation values for all compounds are in the range of 1.2 to 1.4. A saturation value close to unity, *i.e.*, weak voltage bias dependence of the current in the reverse direction, is an indication for an efficient charge separation and extraction. Larger values indicate that recombination losses and field-dependent dissociation of charge-carriers are present.[44,45]

Bulk heterojunction solar cells

BHJ solar cells with a photoactive layer thickness of 20 nm were prepared using oligomers **1–4** as the donor and C_{60} as an acceptor. The blend layer was prepared by co-evaporation of the donor and the acceptor in a ratio of 1 : 1 by volume at a substrate temperature of 70 °C. This substrate temperature was found to be optimal for quaterthiophene-based materials.[25] It has been shown that heating of the substrate should result in a morphology, which provides better charge transport in the active layer.[39,46] All other layers were vacuum-deposited using the following layer sequence: ITO-coated glass substrate, 15 nm C_{60}, 20 nm photoactive blend layer, 5 nm of undoped and 50 nm of p-doped 9,9-bis[4-(*N*,*N*-bis-biphenyl-4-ylamino)phenyl]-9*H*-fluorene (BPAPF) as the hole transport layer (HTL), 1 nm thick NDP9 layer and the Au top electrode (Fig. 7). The data for the BHJ solar cells are summarized in Table 5 and *J–V* characteristics as well as EQE spectra of the solar cells are shown in Fig. 8.

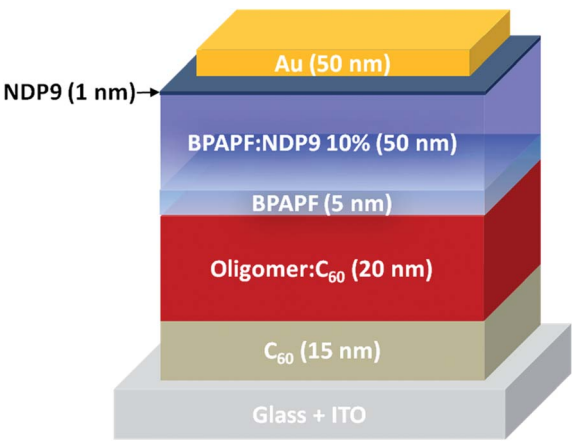

Fig. 7 General device architecture of investigated BHJ solar cells.

Table 5 Photovoltaic parameters of bulk-heterojunction solar cells containing DCV end-capped BDT-derivatives **1–4** and **6** compared to **DCV4T**. The active layer thickness was 20 nm for all devices with an oligomer : C_{60} ratio of 1 : 1 by volume

Compound	J_{SC}[a] [mA cm^{-2}]	V_{OC} [V]	FF [%]	η [%]	Saturation[b]	Intensity [mW cm^{-2}]
DCV4T	7.4	0.96	46	3.2	1.24	102
1	6.0	1.00	60	3.6	1.12	100
2	4.0	1.01	52	2.1	1.18	99
3	5.6	0.99	57	3.2	1.12	100
4	4.6	1.00	61	2.8	1.14	103
6	5.4	0.98	50	2.6	1.10	99

[a] Measured with mask and corrected to 100 mW cm^{-2}. [b] Defined as $J(-1\ V)/J_{SC}$.

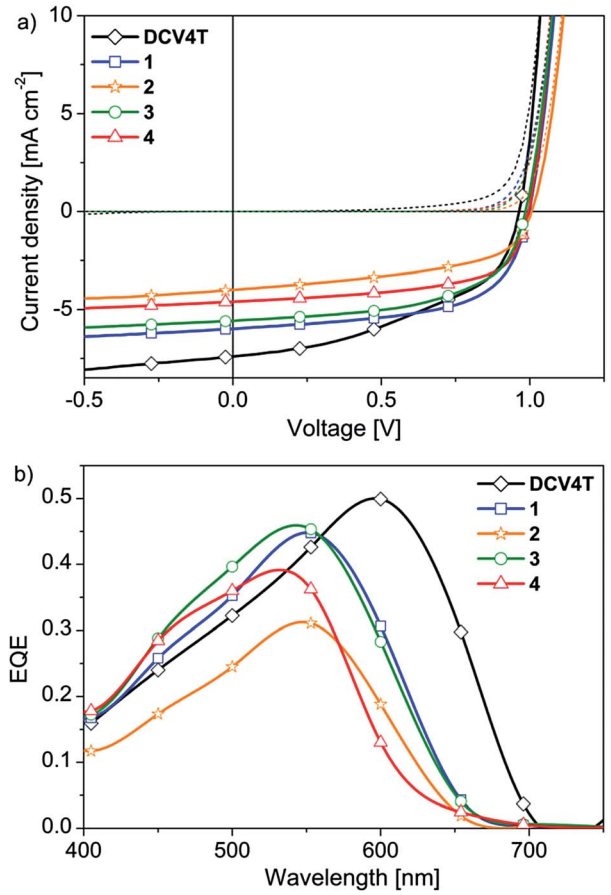

Fig. 8 (a) Representative *J*–*V*-characteristics of bulk-heterojunction solar cells with DCV end-capped benzodithiophene **1** and **DCV4T** as donor materials. (b) Corresponding EQE spectra of BHJ solar cells.

All BDT-containing oligomers gave high V_{OC}s close to 1 V. This was expected, since in BHJ solar cells the V_{OC} is dominated by the LUMO of the acceptor (C_{60}) and the HOMO of the HTL (BPAPF).[40] BHJ solar cells with oligomers **1–4** reached J_{SC}s of 4.0 to 6.0 mA cm^{-2}. Comparing the J_{SC} achieved with all donor materials, the BHJ cells followed the same trend as the PHJ solar cells. The development of the photocurrents correlates well with the EQE-spectra. Oligomers **1–3** showed qualitatively similar spectra with a maximum at around 550 nm. The EQE spectrum of **4** is slightly blue-shifted and corresponds well to the PHJ device and the thin film absorption spectra. The FF besides efficiency is one of the most critical parameter in organic solar cells. Interestingly, the BHJ devices with BDT derivatives **1–4** exhibited higher FFs (52% to 61%), which are significantly higher compared to devices of reference **DCV4T** (46%). This suggests that the molecular planarization in BDTs resulted in an improved charge carrier transport in the donor–acceptor blend layers. Consequently, BHJ cells prepared with BDTs **1–4** showed good efficiencies of 3.6%, 2.1%, 3.2%, and 2.8%. Additionally, the significantly lower saturation values of 1.12 to 1.18 for the BDT-based BHJ cells compared to **DCV4T** (1.24) indicate a decrease of field-dependent recombination of photogenerated charge carriers. It is interesting to note that the best cell in this series incorporating planar BDT-oligomer **1** gave a 12.5% improvement in efficiency compared to reference **DCV4T** (Table 5).

Oligomers **5** and **7** were not tested in BHJSCs due to their low efficiencies in PHJ devices and high degree of decomposition during sublimation. The BHJ device prepared with oligomer **6** gave a J_{SC} of 5.4 mA cm^{-2}, a FF of 50%, and an efficiency of 2.6%. The lower performance of **6** is mainly ascribed to the moderate fill factor.

Conclusions

We have synthesized and characterized a series of novel benzo-[2,1-*b*:3,4-*b*′]dithiophene (BDT)- and naphtho[2,1-*b*:3,4-*b*′]-dithiophene (NDT)-containing oligomers for applications in organic solar cells. Gradient vacuum sublimation led to pure organic semiconducting materials with high thermal stability. Incorporation of the fused central BDT and NDT units resulted in blue-shifted absorption and emission spectra and in an increase of the band gap compared to non-fused reference **DCV4T**. PHJ and BHJ solar cells were fabricated by vacuum-processing using these oligomers as the electron donor and C_{60} as the electron acceptor. PHJ solar cells constructed using all oligomers displayed high V_{OC}s and efficiencies in the range of 1.5–3.0% under full sun illumination. Despite a blue-shifted absorption and a larger band gap, the highest PCE of 3.6% was obtained in BHJ devices for BDT-oligomer **1** which is higher compared to reference **DCV4T**. This improvement is mainly ascribed to the large increase in the V_{OC} and FF values. The current results clearly reveal that the structural concept presented here, *i.e.*, integration of fused-ring systems, represents an interesting direction in the design of novel photoactive materials for solar cell applications.

Experimental

Physical measurements and instrumentation

NMR spectra were recorded on a Bruker AMX 500 (^{1}H NMR: 500 MHz, ^{13}C NMR: 125 MHz) at 100 °C or an Avance 400 spectrometer (^{1}H NMR: 400 MHz, ^{13}C NMR: 100 MHz) at 25 °C unless otherwise noted. Chemical shift values (δ) are expressed in parts per million using residual solvent protons (^{1}H NMR, $\delta_H = 7.26$ for $CDCl_3$; ^{1}H NMR, $\delta_H = 5.92$ for TCE; ^{1}H NMR, $\delta_H = 5.32$ for DCM; ^{13}C NMR, $\delta_C = 77.16$ for $CDCl_3$) as the internal standard. The splitting patterns are designated as follows: s (singlet), d (doublet), t (triplet), q (quartet), and m (multiplet). The assignments are Th-H (thiophene protons), Fu-H (furan protons), Ph-H (phenyl protons), and DCV-H (dicyanovinylene protons). Melting points were determined using a Mettler Toledo DSC 823^e and were not corrected. Elemental analyses were performed on an Elementar Vario EL. Thin layer chromatography was carried out on aluminum plates, pre-coated with silica gel, Merck Si60 F_{254}. Preparative column chromatography was performed on glass columns packed with silica gel, Merck Silica 60, particle size 40–43 μm. Electron impact (EI) mass spectra were recorded on a Varian 3800, chemical ionisation (CI) mass spectra on a Finnigan MAT SSQ-7000 and MALDI-TOF mass spectra on a Bruker Daltonics Reflex III.

Optical measurements in solution were carried out in 1 cm cuvettes with Merck Uvasol grade DCM. Absorption spectra were recorded on a Perkin Elmer Lambda 19 spectrometer and corrected fluorescence spectra were recorded on a Perkin Elmer LS 55 fluorescence spectrometer. Cyclic voltammetry experiments were performed with a computer-controlled Autolab PGSTAT30 potentiostat in a three-electrode single-compartment cell with a platinum working electrode, a platinum wire counter electrode, and an Ag/AgCl reference electrode. All potentials were internally referenced to the ferrocene/ferrocenium couple.

Thin film and device fabrication

Thin films and heterojunction solar cell devices were prepared by thermal vapor deposition in an ultra-high vacuum at a base pressure of 10^{-7} mbar on the substrate at room temperature. Thin films for absorption and emission measurements were prepared on quartz substrates and solar cells on tin-doped indium oxide (ITO) coated glass (Thin Film Devices, USA, sheet resistance of 30 Ω sq^{-1}). Layer thicknesses were determined during evaporation by using quartz crystal monitors calibrated for the respective material. The thin films prepared for absorption and emission measurements are approximately 30 nm thick. The thin film absorption spectra were recorded on a Shimadzu UV-2101/3101 UV-vis spectrometer. The thin film emission spectra were recorded with an Edinburgh Instruments FSP920 fluorescence spectrometer. Bulk-heterojunction solar cells were prepared layer by layer without breaking the vacuum. The layer structure of the bulk-heterojunction solar cells is as follows: ITO; 15 nm C_{60}; 20 nm blend layer of respective benzodithiophenes and C_{60} (ratio of 1 : 1 by volume) prepared by co-evaporation deposited on the heated substrate (70 °C); 5 nm BPAPF; 50 nm BPAPF doped with NDP9 (purchased from Novaled AG Germany, 10 wt%); 1 nm NDP9; 50 nm gold.

Photovoltaic characterization

J–V and EQE measurements were carried out in a glove box under a nitrogen atmosphere. *J–V* characteristics were measured using a source-measure unit (Keithley SMU 2400) and an AM 1.5G sun simulator (KHS Technical Lighting SC1200). The intensity was monitored with a silicon photodiode (Hamamatsu S1337) which was calibrated at Fraunhofer ISE. The mismatch between the spectrum of the sun simulator and the AM 1.5G spectrum was not taken into account. For well-defined active solar cell areas, aperture masks (2.76 mm^2) were used. Simple EQE measurements were carried out using the sun simulator in combination with color filters for monochromatic illumination. The illumination intensities were measured with a silicon reference diode (Hamamatsu S1337).

Materials

Tetrahydrofuran (THF, Merck) was dried under reflux over sodium/benzophenone (Merck). Dimethylformamide (DMF, Merck) was dried under reflux over phosphorous pentoxide (Merck). Dichloromethane (DCM) and *n*-hexane were purchased from Prolabo and distilled prior to use. All synthesis steps were carried out under an argon atmosphere. *n*-Butyl lithium (1.6 N in *n*-hexane) and $Pd_2(dba)_3 \cdot CHCl_3$ were purchased from Acros. Piperidine, triethylamine, acetic anhydride, titanium tetrachloride, β-alanine, acetonitrile, zinc, tetra-*n*-butylammonium fluoride, methyl iodine and chlorobenzene were purchased from Merck. Malononitrile, *o*-dichlorobenzene, trimethyltin chloride and 1,2-dibromo-benzene **28** were purchased from Aldrich. $HP(^tBu)_3BF_4$, cesium carbonate, 5-bromo-2-furaldehyde **14** and *N*,*O*-dimethylhydroxylamine hydrochloride **17** were purchased from Afla (Aesar). Tetrakis(triphenyl-phosphine) palladium ($Pd(PPh_3)_4$) was synthesized according to a literature-known process.[47]

Benzo[2,1-*b*:3,4-*b*′]dithiophene **8**,[27] 2-[(5-bromothien-2-yl)-methylene]malononitrile **10**,[24] 5-bromo-4-butylthiophene-2-carbaldehyde **11**,[26] 2-[(5-bromo-3,4-dimethylthien-2-yl)-methylene]-malononitrile **13**,[25] (3,3′-dibromo-[2,2′-bithien]-5,5′-diyl)bis-(trimethylsilane) **19**, and benzo[2,1-*b*:3,4-*b*′]dithiophene-4,5-dione **23** (ref. 30) were synthesized as described in the literature.

Synthesis

2,7-Bis(trimethylstannyl)benzo[2,1-*b*:3,4-*b*′]dithiophene (9). Benzo[2,1-*b*:3,4-*b*′]dithiophene **8** (353 mg, 1.86 mmol) was dissolved in 6.3 mL of dry THF. The solution was degassed three times and was cooled to −78 °C. *n*-BuLi (2.56 mL, 4.08 mmol, 1.6 M in hexane) was added over 7 minutes whereupon a grey suspension was formed. The suspension was stirred for 1 h at −78 °C and 2.5 h at room temperature. After cooling to −78 °C again, trimethylstannyl chloride (814 mg, 4.08 mmol) in 2.0 mL THF was added in one portion. The mixture was stirred for 1 h at −78 °C and at room temperature overnight. A light yellow solution was formed. 35 mL of *n*-hexane were added. The white suspension was washed with 3 × 50 mL water, dried over Na_2SO_4, and the solvent was removed. After drying in a high vacuum, product **9** (938 mg, 1.75 mmol, purity: 96% (^{1}H-NMR))

was obtained as a white solid. ^{1}H NMR (400 MHz, $CDCl_3$): δ = 7.73 (s, 1H, Th-H), 7.50 (s, 1H, Ph-H), 0.45 (s, 9H, Sn–CH_3). ^{13}C NMR (100 MHz, CD_2Cl_2): δ = 138.24, 138.11, 138.02, 132.93, 120.01, −8.10. MS (EI): m/z = 514 $[M - H]^+$, 502 $[M - CH_3]^+$. The product was used without further purification and analytical data were in agreement with the literature.[48]

2-[(5-Bromo-4-butylthien-2-yl)methylene]malononitrile (12). 5-Bromo-4-butylthiophene-2-carbaldehyde **11** (250 mg, 1.01 mmol), malononitrile (134 mg, 2.02 mmol), and β-alanine (4.5 mg, 57 μmol) were dissolved in 10 mL ethanol and heated to reflux for 15 h. The reaction mixture was cooled to room temperature and 20 mL diethyl ether was added. The reaction mixture was washed with water (6 × 20 mL) and dried over Na_2SO_4. The removal of the solvent yielded 335 mg of a brown solid, which was purified by column chromatography (silica; *n*-hexane–DCM 1 : 1) and pure product **12** (302 mg, 1.03 mmol, 90%) was obtained as an orange solid. ^{1}H NMR (400 MHz, $CDCl_3$): δ = 7.68 (s, 1H, DCV-H), 7.42 (s, 1H, Th-H), 2.65–2.57 (m, 2H, –CH_2–), 1.63–1.52 (m, 2H, –CH_2–), 1.41–1.32 (m, 2H, –CH_2–), 0.94 (t, ^3J = 7.3 Hz, 4H, –CH_3). ^{13}C NMR (100 MHz, $CDCl_3$): δ = 150.15, 144.83, 138.96, 134.96, 124.33, 113.90, 31.66, 29.01, 22.34, 13.93. MS (EI): m/z = 296 $[M]^+$, 253 $[M - C_3H_7]^+$. Elemental analysis: calc. (%) for $C_{12}H_{11}BrN_2S$: C 48.82; H 3.76; N 9.49; S 10.86; found: C 49.06; H 3.77; N 9.51; S 10.67.

2-[(5-Bromofuran-2-yl)methylene]malononitrile (15). 5-Bromofuran-2-carbaldehyde **14** (1.00 g, 5.71 mmol) and malononitrile (0.76 g, 11.4 mmol) were suspended in 40 mL dichloroethane and degassed. Piperidine (30.0 μL, 0.57 mmol) was added and degassed again. The solution was heated to reflux for 20 h. The reaction mixture was cooled to room temperature and the solvent was removed. The residue was recrystallized from ethanol and pure product **15** (828 mg, 3.71 mmol, 65%) was obtained as a brown crystalline solid. M.p.: 155.1–159.1 °C, ^{1}H NMR (400 MHz, $CDCl_3$): δ = 7.41 (s, 1H, DCV-H), 7.35 (d, 1H, ^3J = 3.8 Hz, furan-H4), 6.67 (d, 1H, ^3J = 3.8 Hz, furan-H3). ^{13}C NMR (100 MHz, $CDCl_3$): δ = 149.88, 141.67, 132.64, 124.84, 113.64, 112.45, 116.81, 77.98. MS (EI): m/z = 224 $[M]^+$. Elemental analysis: calc. (%) for $C_8H_3BrN_2O$: C 43.08; H 1.36; N 12.56; found: C 43.35; H, 1.43, N: 12.63.

***N*-Methoxy-*N*-methylacetamide (18).** *N*,*O*-Dimethylhydroxylamine hydrochloride **17** (12.0 g, 0.12 mol) hydrochloride was suspended under nitrogen in 120 mL DCM and cooled to 0 °C. Triethylamine (35.8 mL, 0.26 mol) and acetyl chloride **16** (9.22 mL, 0.13 mol) were successively added within 45 min, and the temperature reached 20 °C despite ice cooling. Stirring at 0 °C was continued for 1 h and stirring without cooling was continued for 2 h. 120 mL of water was added to the suspension and the organic phase was washed with 2 × 50 mL 1 N HCl, and with 50 mL sat. NaCl, dried over Na_2SO_4, and the solvent was removed. Distillation under reduced pressure gave a colorless oil of **18** (5.6 g, 50 mmol, 44%). B.p. 50 °C (18 mbar), ^{1}H NMR (400 MHz, $CDCl_3$): δ = 3.60 (s, 3H, O–CH_3), 3.17 (s, 3H, N–CH_3), 2.12 (s, 3H, CH_3). ^{13}C NMR (100 MHz, $CDCl_3$): δ = 171.74, 60.93, 31.75, 19.62. MS (EI): m/z = 103 $[M]^+$, elemental analysis: calc. (%) for $C_4H_9NO_2$: C 46.59; H 8.80; N 13.58; found: C 46.67; H, 8.76, N: 13.58. Analytical data were in accordance with the literature.[29,49]

1,1′-[5,5′-Bis(trimethylsilyl)-[2,2′-bithien]-3,3′-diyl]diethanone (20). (3,3′-Dibromo-[2,2′-bithien]-5,5′-diyl)bis(trimethylsilane) **19** (2.0 g, 4.2 mmol) was dissolved in 44 mL dry THF and cooled to −78 °C. *n*-BuLi (5.8 mL, 9.32 mmol, 1.6 M in hexane) was added within 15 minutes. The mixture was stirred for 45 minutes at −78 °C and then *N*-methoxy-*N*-methylacetamide **18** (961 mg, 9.32 mmol) was added. The reaction mixture was allowed to stir for 2 h at −78 °C and was warmed to room temperature overnight. The reaction was quenched with 50 mL saturated $NaHCO_3$ solution. The product was extracted with DCM, the organic solution was dried over Na_2SO_4, filtered off, and the solvent was removed. The crude product was purified by column chromatography (flash silica; DCM) to obtain pure **20** (1.10 g, 2.79 mmol; 66%) as a slightly yellow solid. M.p. 84.0–85.2 °C, ^{1}H NMR (400 MHz, $CDCl_3$): δ = 7.57 (s, 2H, Th-H), 3.28 (s, 6H, CH_3), 0.35 (s, 18H, Si–CH_3), ^{13}C NMR (100 MHz, $CDCl_3$): δ = 193.84, 144.04, 142.55, 141.52, 135.75, 29.32, 0.12. MS (EI): m/z = 394 $[M]^+$, 352 $[M - (CH_3)_3]^+$, elemental analysis: calc. (%) for $C_{18}H_{26}O_2S_2Si_2$: C 54.77; H 6.64; S 16.25; found: C 54.92; H 6.71, S 16.10.

4,5-Dimethylbenzo[2,1-*b*:3,4-*b*′]dithiophene (21). 90 mL dry THF was cooled to −10 °C and $TiCl_4$ (1.4 mL, 10 mmol) was added dropwise. Zinc powder (1.6 g, 20 mmol) was added in a nitrogen atmosphere and the mixture stirred for 2 h at 0 °C. A solution of 1,1′-[5,5′-bis(trimethylsilyl)-[2,2′-bithien]-3,3′-diyl] diethanone **20** (500 mg, 1.27 mmol) in 60 mL dry THF was added very slowly under reflux. After addition, reflux was continued for further 12 h. The mixture was cooled to 0 °C and aqueous 5 wt% $NaHCO_3$ was successively added. THF was removed under reduced pressure and the mixture was extracted with DCM. The extract was dried over Na_2SO_4 and filtered off. After evaporation of the solvent a yellow solid was obtained. This was dissolved in 20 mL THF and TBAF (1.6 g, 10 mmol) was added as a solid. After stirring for 15 min at room temperature the reaction was quenched with 25 mL water and THF was removed. The product was extracted with 3 × 30 mL DCM, dried over Na_2SO_4, and filtered off. The crude product was purified by column chromatography (flash silica; *n*-hexane) and white crystals of **21** (170 mg, 0.78 mmol; 66%) were obtained as a pure product. M.p. 114.6–115.6 °C, ^{1}H NMR (400 MHz, $CDCl_3$): δ = 7.49 (d, ^3J = 5.5 Hz, 2H, Th-H), 7.39 (d, ^3J = 5.4 Hz, 2H, Th-H), 2.64 (s, 6H, CH_3), ^{13}C NMR (100 MHz, $CDCl_3$): δ = 137.95, 130.98, 126.99, 123.67, 123.58, 16.46, MS (EI): m/z = 220 $[M + 2H]^+$; 205 $[M - CH_3]^+$, elemental analysis: calc. (%) for $C_{12}H_{10}S_2$: C 66.01; H 4.62; S 29.37; found: C 65.95; H 4.74; S 29.19.

2,7-Bis(trimethylstannyl)-4,5-dimethylbenzo[2,1-*b*:3,4-*b*′]-dithiophene (22). 4,5-Dimethylbenzo[2,1-*b*:3,4-*b*′]dithiophene **21** (120 mg, 0.55 mmol) was dissolved in 2.3 mL dry THF and was degassed three times. The solution was cooled to −78 °C and *n*-BuLi (0.76 mL, 1.21 mmol, 1.6 M in hexane) was added over a few minutes whereupon a white suspension was formed. The suspension was stirred for 1 h at −78 °C and 2.5 h at room temperature. After cooling to −78 °C trimethylstannyl chloride (241 mg, 1.21 mmol) in 1.5 mL THF was added in one portion. The mixture was stirred for 1 h at −78 °C and at room temperature overnight. 35 mL of *n*-hexane were added. The white suspension was washed with

3 × 50 mL water, dried over Na_2SO_4, and the solvent was removed in a vacuum. A white solid of **22** was obtained, which was dried in a high vacuum. The product (280 mg, 0.48 mmol, 88%) was used in the next step without further purification. ^{1}H NMR (400 MHz, $CDCl_3$): δ = 7.53 (s with ^{13}C-satellites, $^1J_{C-H}$ = 28.5 Hz, 2H, Th-H), 2.65 (s, 6H, CH_3), 0.45 (s with Sn-satellites, $^2J_{Sn119-H}$ = 57.6 Hz, $^2J_{Sn117-H}$ = 55.2 Hz, 18H, Sn–CH_3), ^{13}C NMR (100 MHz, $CDCl_3$): δ = 138.50, 137.10, 135.31, 131.53, 126.09, 16.51, −8.07.

Benzo[2,1-*b*:3,4-*b*′]dithiene-4,5-diyl diacetate (24). 15 mL of dry DCM were added to a tube containing benzo[2,1-*b*:3,4-*b*′]-dithiophene-4,5-dione **23** (269 mg, 1.22 mmol) and Zn dust (0.84 g, 12.8 mmol). Acetic anhydride (1.21 mL, 12.8 mmol) and triethylamine (2.5 mL, 18 mmol) were syringed in. The mixture was stirred at 25 °C overnight and then filtered through Celite. The filtrate was washed with 50 mL brine, 50 mL 2 M HCl and with 2 × 50 mL saturated $NaHCO_3$. The organic layer was dried over Na_2SO_4, filtered, treated with activated charcoal, and filtered again two times through Celite. Removal of the solvent under reduced pressure and further drying under high vacuum led to a slightly red crystalline solid. Pure product **24** was obtained (210 mg, 0.69 mmol, 57%) by recrystallization from ethanol. M.p. 205.1–206.5 °C, ^{1}H NMR (400 MHz, $CDCl_3$): δ = 7.44 (d, ^3J = 5.5 Hz, 2H, Th-H), 7.29 (d, ^3J = 5.5 Hz, 2H, TH-H), 2.44 (s, 6H, –CH_3), ^{13}C NMR (100 MHz, $CDCl_3$): δ = 168.39, 126.10, 121.37, 77.48, 76.84, 20.69, MS (GC): m/z = 306 $[M]^+$, elemental analysis: calc. (%) for $C_{14}H_{10}O_4S_2$: C 54.89; H 3.29; S 20.93; found: C 54.76; H 3.40; S 21.11. Analytical data were in accordance with the literature.[50]

4,5-Dimethoxybenzo[2,1-*b*:3,4-*b*′]dithiophene (25). Benzo[2,1-*b*:3,4-*b*′]dithien-4,5-diyl diacetate **24** (400 mg, 1.31 mmol), cesium carbonate (2.13 g, 6.53 mmol), and methyl iodide (0.4 mL, 6.5 mmol) were dissolved in 20 mL acetonitrile. The reaction mixture was stirred at 75 °C. After three days, GC/MS analysis showed the presence of intermediate. Therefore, methyl iodide (0.4 mL, 6.5 mmol) and cesium carbonate (2.13 g, 6.53 mmol) were added and the mixture was heated to 75 °C for further 24 h. GC/MS analysis showed full conversion; the mixture was cooled to room temperature and acetonitrile was removed by rotary evaporation. The residue was partitioned between water and dichloromethane. The organic phase was washed with 2 × 100 mL 1 M HCl and then with 100 mL water, dried over N_2SO_4 and filtered off. Evaporation of the solvent led to a brown oil. The crude product was purified by column chromatography (flash-silica; *n*-hexane–DCM 1 : 1). Pure product **25** (282 mg, 1.13 mmol, 86%) was obtained as a white solid. M.p. 41.0–41.6 °C, ^{1}H NMR (400 MHz, $CDCl_3$): δ = 7.52 (d, ^3J = 5.4 Hz, 2H, Th-H), 7.37 (d, ^3J = 5.3 Hz, 2H, Th-H), 4.06 (s, 6H, O–CH_3), ^{13}C NMR (100 MHz, $CDCl_3$): δ = 144.18, 133.87, 129.52, 124.54, 121.91, 61.78, MS (GC): m/z = 250 $[M]^+$, elemental analysis: calc. (%) for $C_{12}H_{10}O_2S_2$: C 57.57; H 4.03; S 25.62; found: C 57.75; H 4.13; S 25.83.

2,7-Bis(trimethylstannyl)-4,5-dimethoxybenzo[2,1-*b*:3,4-*b*′]-dithiophene (26). 4,5-Dimethoxybenzo[2,1-*b*:3,4-*b*′]dithiophene **25** (345 mg, 1.28 mmol) was dissolved in 4.7 mL dry THF and was degassed three times. The slightly yellow solution was cooled to −78 °C and *n*-BuLi (2.0 mL, 3.2 mmol, 1.6 M in hexane) was added over 20 minutes whereupon a grey suspension was formed. The suspension was stirred for 1.5 h at −78 °C and 1.5 h at room temperature. After cooling to −78 °C again, trimethylstannyl chloride (632 mg, 3.20 mmol) in 1.0 mL THF was added in one portion. The mixture was stirred for 1 h at −78 °C and at room temperature overnight. A light yellow solution was formed and 35 mL of *n*-hexane were added. The white suspension was washed with 3 × 50 mL water, dried over Na_2SO_4 and the solvent was removed in a vacuum. The crude product was dried in high vacuum to obtain 780 mg (1.24 mmol, 92%) of a white solid of **26**, which was used in the next step without further purification. ^{1}H NMR (400 MHz, $CDCl_3$): δ = 7.56 (s with ^{13}C-satellites, $^1J_{C-H}$ = 28.2 Hz, 2H, Th-H), 4.06 (s with ^{13}C-satellites, 6H, OCH_3), 0.45 (s with Sn-satellites, $^2J_{Sn119-H}$ = 57.8 Hz, $^2J_{Sn117-H}$ = 55.2 Hz, 18H, Sn–CH_3), ^{13}C NMR (100 MHz, $CDCl_3$): δ = 143.48, 138.74, 134.66, 129.47, 61.74 (s), −8.06 (s).

[3,3′-Bis(trimethylstannyl)-[2,2′-bithien]-5,5′-diyl]bis(trimethylsilane) (27). 3,3′-Dibromo-5,5′-bis(trimethylsilyl)-2,2′-bithiophene **19** (1.03 g, 2.20 mmol) was dissolved in 7.5 mL dry THF and degassed five times. The solution was cooled to −78 °C and *n*-BuLi (3.01 mL, 4.82 mmol, 1.6 M in hexane) was added over eight minutes. The solution was stirred for 30 minutes at −78 °C and was quenched with trimethylstannyl chloride (961 mg, 4.82 mmol) in 2.0 mL THF. The mixture was stirred for 2 h at −78 °C and overnight at room temperature. 15 mL of *n*-hexane were added and the organic solution was washed with 4 × 50 mL water, dried over Na_2SO_4, and the solvent was removed in a vacuum. The crude product was dried in high vacuum. Recrystallization from ethanol led to pure **27** (280 mg, 0.48 mmol, 88%) as a slightly yellow crystalline solid. M.p. 103.9–104.6 °C, ^{1}H NMR (400 MHz, $CDCl_3$): δ = 7.16 (s with C-satellites, $^1J_{C-H}$ = 14.6 Hz, 2H, Th-H), 0.34 (s with Si-satellites, $^2J_{Si-H}$ = 6.7 Hz, 18H, Si–CH_3), 0.11 (s with Sn-satellites, $^2J_{Sn119-H}$ = 56.7 Hz, $^2J_{Sn117-H}$ = 54.0 Hz, 18H, Sn–CH_3), ^{13}C NMR (100 MHz, $CDCl_3$): δ = 148.96, 142.32, 141.22, 140.35, 0.25 (s with Si-satellites, $^1J_{Si-C}$ = 50.1 Hz), −8.04 (s with Sn-satellites, $^1J_{Sn119-C}$ = 362.1 Hz, $^1J_{Sn117-C}$ = 346.1 Hz), MS (EI): m/z = 622 $[M - CH_3]^+$, elemental analysis: calc. (%) for $C_{20}H_{38}S_2Si_2Sn_2$: C 37.76; H 6.02; S 10.08; found: C 37.90; H 6.30; S 10.17.

Naphtho[2,1-*b*:3,4-*b*′]dithiophene (29). 3,3′-Di(trimethylstannyl)-5,5′-bis(trimethylsilyl)-2,2′-bithiophene **27** (752 mg, 1.14 mmol) was dissolved in 11.5 mL DMF and the solution was degassed. 1,2-Dibromobenzene **28** (140 μL, 1.14 mmol), $Pd_2(dba)_3 \cdot CHCl_3$ (60 mg, 58 μmol), and $HP(^tBu)_3BF_4$ (67.0 mg, 231 μmol) were added and the mixture was degassed again. The mixture was heated to 120 °C for 2 days. The mixture was cooled to room temperature, quenched with water, and the product was extracted with DCM. The organic solution was washed with 2 × 50 mL sat. $NaHCO_3$, 2 × 50 mL brine, and with water, dried over Na_2SO_4, and filtered off. Evaporation of the solvent under reduced pressure led to a slightly yellow oil. The oil was redissolved in 10 mL THF and TBAF (0.8 g, 2.5 mmol) was added. After stirring for 15 minutes at room temperature the reaction mixture was quenched with 10 mL of saturated $NaHCO_3$ solution. The product was extracted with 3 × 30 mL DCM. The organic solution was washed with 2 × 30 mL saturated $NaHCO_3$

and water, dried over Na_2SO_4, and filtered off. Evaporation of the solvent under reduced pressure led to a slightly yellow oil. The crude product was purified by column chromatography (flash silica; *n*-hexane–ethyl acetate 50 : 1) and a white crystalline solid of **29** (145 mg, 0.60 mmol; 53%) was obtained as a pure product. M.p. 166.5–167.6 °C. ^{1}H NMR (400 MHz, $CDCl_3$): 8.42–8.36 (m, 2H, Ph-H), 8.01 (d, ^3J = 5.3 Hz, 2H, Th-H), 7.67–7.60 (m, 2H, Ph-H), 7.52 (d, ^3J = 5.3 Hz, 2H, Th-H). ^{13}C NMR (100 MHz, $CDCl_3$): δ = 134.49, 132.19, 127.77, 125.94, 124.50, 123.93, 122.96. MS (EI): m/z = 240 $[M]^+$. Elemental analysis: calc. (%) for $C_{14}H_8S_2$: C, 69.96; H, 3.36; S, 26.68; found: C, 70.00; H, 3.49; S, 26.40. Analytical data were in agreement with the literature.[51]

2,9-Bis(trimethylstannyl)naphtho[2,1-*b*:3,4-*b*′]dithiophene (30). Naphtho[2,1-*b*:3,4-*b*′]dithiophene **29** (191 mg, 0.79 mmol) was dissolved in 4.5 mL of dry THF. The solution was degassed three times and was cooled to −78 °C. *n*-BuLi (1.10 mL, 1.75 mmol, 1.6 M in hexane) was added slowly whereupon a grey suspension was formed. The suspension was stirred for 1.5 h at −78 °C and 2.5 h at room temperature. After cooling to −78 °C again, trimethylstannyl chloride (396 mg, 1.99 mmol) in 1.1 mL THF was added in one portion. The mixture was stirred for 1.5 h at −78 °C and at room temperature overnight. A light yellow solution was formed. 35 mL of *n*-hexane were added. The white suspension was washed with 3 × 50 mL water, dried over Na_2SO_4, and the solvent was removed. After drying in high vacuum, product **30** (purity: 92% (GC) 457 mg, 0.74 mmol, 94%) was obtained as a brownish oil. ^{1}H NMR (400 MHz, $CDCl_3$): δ = 8.51–8.47 (m, 2H, Ph-H), 7.12 (s with C-satellites, $^1J_{C-H}$ = 27.35 Hz, 2H, Th-H), 7.67–7.63 (m, 2H, Ph-H), 0.56 (s with Sn-satellites, $^2J_{Sn119-H}$ = 57.62 Hz, $^2J_{Sn117-H}$ = 55.22 Hz, 18H, Sn–CH_3), the product was used without further purification.

2,2′-{[5,5′-(Benzo[2,1-*b*:3,4-*b*′]dithien-2,7-diyl)bis(thien-5,2-diyl)]bis(methan-1-yl-1-yl-idene)}dimalononitrile (1). A mixture of 2,7-bis(trimethylstannyl)benzo[2,1-*b*:3,4-*b*′]dithiophene **9** (380 mg, 0.69 mmol), 2-[(5-bromothien-2-yl)methylene]malononitrile **10** (381 mg, 1.60 mmol), and $Pd(PPh_3)_4$ (72 mg, 62 μmol) in 18 mL dry DMF was heated to 80 °C for 12 h. After cooling, the resulting precipitate was filtered off and washed several times with methanol and *n*-hexane. After drying, oligomer **1** (283 mg, 0.60 mmol, 81%) was obtained as a deep red solid. The product was further purified by gradient vacuum sublimation. M.p. 350 °C. ^{1}H NMR (500 MHz, DMSO-d_6): δ = 8.59 (s, 2H, DCV-H), 8.13 (s, 2H, Th-H), 7.98 (d, ^3J = 4.1 Hz, 2H, Th-H), 7.95 (s, 2H, Ph-H), 7.75 (d, ^3J = 4.1 Hz, 2H, Th-H). ^{13}C NMR (100 MHz, $CDCl_3$): δ = 151.51, 146.10, 140.76, 138.34, 134.38, 133.32, 132.02, 126.56, 124.84, 121.89, 113.72, 113.10, 75.51. MS (CI): m/z = 506 $[M]^+$ (calcd for $C_{26}H_{10}N_4S_4$: 505.98). Elemental analysis: calc. (%) for $C_{26}H_{10}N_4S_4$: C, 61.64; H, 1.99; N, 11.06; S, 25.31; found: C, 61.77; H, 2.18; N, 11.15; S, 25.36.

2,2′-{[5,5′-(Benzo[2,1-*b*:3,4-*b*′]dithien-2,7-diyl)bis(4-butylthien-5,2-diyl)]bis(methan-1-yl-1-yl-idene)}dimalononitrile (2). A mixture of 2,7-bis(trimethylstannyl)benzo[2,1-*b*:3,4-*b*′]dithiophene **9** (214 mg, 0.39 mmol), 2-((5-bromo-4-butylthien-2-yl) methylene)malononitrile **12** (252 mg, 0.85 mmol) and $Pd(PPh_3)_4$ (44 mg, 38 μmol) in 10 mL dry DMF was heated to 80 °C for 15 h. After cooling, the resulting precipitate was filtered off and washed several times with water, methanol, acetone and *n*-hexane. After drying, oligomer **2** (188 mg, 0.34 mmol, 87%) was obtained as a deep purple solid. The product was further purified by column chromatography (flash silica, DCM). M.p. 311 °C (DSC). ^{1}H NMR (500 MHz, DMSO-d_6): δ = 8.51 (s, 2H, DCV-H), 8.00 (s, 2H, Th-H), 7.95 (s, 2H, Th-H), 7.90 (s, 2H, Ph-H), 2.98–2.94 (m, 4H, –CH_2–), 1.76–1.64 (m, 4H, –CH_2–), 1.47–1.40 (m, 4H, –CH_2–), 0.94 (t, ^3J = 7.3 Hz, 6H, –CH_3). ^{13}C NMR: solubility not sufficient. MS (MALDI-TOF): m/z = 618.0 $[M^+]$ (calc. for $C_{34}H_{26}N_4S_4$: 618.10). Elemental analysis: calc. (%) for $C_{34}H_{26}N_4S_4$: C, 65.99; H, 4.23; N, 9.05; S, 20.73; found: C, 65.72; H, 4.26; N, 8.97; S, 20.76.

2,2′-{[5,5′-(Benzo[2,1-*b*:3,4-*b*′]dithien-2,7-diyl)bis(3,4-dimethylthien-5,2-diyl)]bis-(methan-1-yl-1-ylidene)}dimalononitrile (3). A mixture of 2,7-bis(trimethylstannyl)benzo[2,1-*b*:3,4-*b*′]-dithiophene **9** (390 mg, 0.73 mmol), 2-[(5-bromo-3,4-dimethlythien-2-yl)methylene]malononitrile **13** (457 mg, 1.71 mmol) and $Pd(PPh_3)_4$ (68 mg, 59 μmol) in 18 mL dry DMF was heated to 80 °C for 15 h. After cooling, the resulting precipitate was filtered off and washed several times with methanol and *n*-hexane. After drying, oligomer **3** (283 mg, 0.60 mmol, 81%) was obtained as a deep red solid. The product was further purified by Soxhlet-extraction with chlorobenzene. M.p. could not be determined due to the decomposition of **3** before melting. ^{1}H NMR (500 MHz, TCE-d_2): δ = 7.96 (s, 2H, DCV-H), 7.90 (s, 2H, Th-H), 7.68 (s, 2H, Ph-H), 2.45 (s, 2H, –CH_3), 2.35 (s, 2H, –CH_3). ^{13}C NMR: solubility not sufficient. MS (MALDI-TOF): m/z = 562.0 $[M^+]$ (calc. for $C_{30}H_{18}N_4S_4$: 562.04). Elemental analysis: calc. (%) for $C_{30}H_{18}N_4S_4$: C, 64.03; H, 3.22; N, 9.96; S, 22.79; found: C, 64.13; H, 3.25; N, 10.14; S, 22.54.

2,2′-{[5,5′-(Benzo[2,1-*b*:3,4-*b*′]dithien-2,7-diyl)bis(furan-5,2-diyl)]bis(methan-1-yl-1-ylidene)}dimalononitrile (4). A mixture of 2,7-bis(trimethylstannyl)benzo[2,1-*b*:3,4-*b*′]dithiophene **9** (355 mg, 0.67 mmol), 2-((5-bromofuran-2-yl)methylene)malononitrile **15** (350 mg, 1.57 mmol) and $Pd(PPh_3)_4$ (42 mg, 36 μmol) in 17 mL DMF was heated to 80 °C for 15 h. After cooling, the resulting precipitate was filtered off and washed several times with water, methanol, acetone and *n*-hexane. After drying, oligomer **4** (286 mg, 0.60 mmol, 90%) was obtained as a deep purple solid. The product was further purified by Soxhlet-extraction with chlorobenzene. M.p. 386 °C. ^{1}H NMR (500 MHz, DMSO-d_6): δ = 8.18 (s, 2H, DCV-H), 8.15 (s, 2H, Th-H), 7.99 (s, 2H, Ph-H), 7.60 (d, ^3J = 3.9 Hz, 2H, Fu-H), 7.43 (d, ^3J = 3.9 Hz, 2H, Fu-H). ^{13}C NMR: solubility not sufficient. MS (CI): m/z = 475 $[M + H]^+$(calc. for $C_{26}H_{10}N_4O_4S_2$: 474.02). Elemental analysis: calc. (%) for $C_{26}H_{10}N_4O_2S_4$: C, 65.81; H, 2.12; N, 11.81; S, 13.51; found: C, 65.72; H, 2.20; N, 11.69; S, 13.33.

2,2′-{[5,5′-(4,5-Dimethylbenzo[2,1-*b*:3,4-*b*′]dithien-2,7-diyl)-bis(thien-5,2-diyl)]-bis(methan-1-yl-1-yl-idene)]}dimalononitrile (5). A mixture of 4,5-dimethylbenzo[2,1-*b*:3,4-*b*′]dithien-2,7-diyl-bis(trimethylstannane) **22** (275 mg, 0.51 mmol), 2-[(5-bromothien-2-yl)methylene]malononitrile **10** (278 mg, 1.16 mmol), and $Pd(PPh_3)_4$ (53 mg, 46 μmol) in 15 mL DMF was heated to 90 °C for 24 h. After cooling, the resulting precipitate was filtered off and washed several times with methanol, acetone and *n*-hexane. After drying, oligomer **5** (252 mg, 0.47 mmol, 93%) was obtained as a black solid. The product was further purified by gradient vacuum sublimation. NMR spectra cannot

be recorded due to poor solubility. M.p. 458 °C. MS (MALDI-TOF): $m/z = 534.1$ [M^+] (calc. for $C_{28}H_{14}N_4S_4$: 534.01). ^{1}H NMR and ^{13}C NMR: solubility not sufficient. Elemental analysis: calc. (%) for $C_{28}H_{14}N_4S_4$: C, 62.90; H, 2.64; N, 10.48; S, 23.99; found: C, 63.13; H, 2.78; N, 10.39; S, 24.17.

2,2′-{[5,5′-(4,5-Dimethoxybenzo[2,1-*b*:3,4-*b*′]dithien-2,7-diyl)-bis(thien-5,2-diyl)]-bis(methan-1-yl-1-yl-idene)}dimalononitrile (6). A mixture of 2,7-bis(trimethylstannyl)-4,5-dimethoxybenzo [2,1-*b*:3,4-*b*′]dithiophene **26** (750 mg, 0.1.18 mmol), 2-[(5-bromothien-2-yl)methylene]malononitrile **10** (651 mg, 2.72 mmol) and $Pd(PPh_3)_4$ (124 mg, 107 mol) in 37 mL DMF was heated to 90 °C for 15 h. After cooling, the resulting precipitate was filtered off and washed several times with methanol, acetone and *n*-hexane. After drying, oligomer **6** (558 mg, 0.98 mmol, 83%) was obtained as a dark purple solid. The product was further purified by gradient vacuum sublimation. M.p. 404 °C. ^{1}H NMR (500 MHz, DMSO-d_6): $\delta = 8.67$ (s, 2H, DCV-H), 8.10 (s, 2H, Th-H), 8.03 (d, $^3J = 3.9$ Hz, 2H, Th-H), 7.89 (d, $^3J = 4.2$ Hz, 2H, Th-H), 4.13 (s, 6H, –O–CH_3). ^{13}C NMR: solubility not sufficient. MS (MALDI-TOF): $m/z = 566.3$ [M^+] (calc. for $C_{28}H_{14}N_4O_2S_4$: 566.0). Elemental analysis: calc. (%) for $C_{28}H_{14}N_4O_2S_4$: C, 59.34; H, 2.49; N, 9.89; S, 23.63; found: C, 59.36; H, 2.54; N, 9.77; S, 23.49.

2,2′-{[5,5′-(Naphtho[2,1-*b*:3,4-*b*′]dithien-2,9-diyl)bis(thien-5,2-diyl)]bis(methan-1-yl-1-yl-idene)}dimalononitrile (7). A mixture of 2,9-bis(trimethylstannyl)naphtho[2,1-*b*:3,4-*b*′]dithiophene **30** (420 mg, 0.68 mmol), 2-[(5-bromothien-2-yl)methylene]malononitrile **10** (376 mg, 1.57 mmol) and $Pd(PPh_3)_4$ (40 mg, 34 μmol) in 30 mL DMF was heated to 90 °C for 24 h. After cooling, the resulting precipitate was filtered off and washed several times with methanol, acetone, *n*-hexane and DCM. After drying, oligomer **7** (363 mg, 0.65 mmol, 96%) was obtained as a black solid. The product was further purified by gradient vacuum sublimation. NMR spectra could not be recorded due to poor solubility. M.p. 473 °C. MS (MALDI-TOF): $m/z = 556.2$ [M^+] (calc. for $C_{30}H_{12}N_4S_4$: 555.99). ^{1}H NMR and ^{13}C NMR: solubility not sufficient. Elemental analysis: calc. (%) for $C_{30}H_{12}N_4S_4$: C, 64.72; H, 2.17; N, 10.06; S, 23.04; found: C, 64.84; H, 2.28; N, 9.96; S, 22.93.

Acknowledgements

We would like to thank the German Ministry of Education and Research (BMBF) for financial support in the frame of project OPEG 2010.

References

1 A. Mishra and P. Bäuerle, *Angew. Chem., Int. Ed.*, 2012, **51**, 2020.
2 K. Walzer, B. Männig, M. Pfeiffer and K. Leo, *Chem. Rev.*, 2007, **107**, 1233.
3 B. Walker, C. Kim and T.-Q. Nguyen, *Chem. Mater.*, 2011, **23**, 470.
4 Y. Chen, X. Wan and G. Long, *Acc. Chem. Res.*, 2013, **46**, 2645.
5 J. Zhou, Y. Zuo, X. Wan, G. Long, Q. Zhang, W. Ni, Y. Liu, Z. Li, G. He, C. Li, B. Kan, M. Li and Y. Chen, *J. Am. Chem. Soc.*, 2013, **135**, 8484.
6 V. Gupta, A. K. K. Kyaw, D. H. Wang, S. Chand, G. C. Bazan and A. J. Heeger, *Sci. Rep*, 2013, **3**, 1965.
7 Y. Liu, C.-C. Chen, Z. Hong, J. Gao, Y. Yang, H. Zhou, L. Dou, G. Li and Y. Yang, *Sci. Rep*, 2013, **3**, 3356.
8 http://www.heliatek.com and http://www.uni-ulm/nawi/oc2.de, accessed February 18th, 2014.
9 J. E. Coughlin, Z. B. Henson, G. C. Welch and G. C. Bazan, *Acc. Chem. Res.*, 2014, **47**, 257.
10 W. Wu, Y. Liu and D. Zhu, *Chem. Soc. Rev.*, 2010, **39**, 1489.
11 K. Takimiya, S. Shinamura, I. Osaka and E. Miyazaki, *Adv. Mater.*, 2011, **23**, 4347.
12 A. R. Murphy and J. M. J. Fréchet, *Chem. Rev.*, 2007, **107**, 1066.
13 M. Liu, R. Rieger, C. Li, H. Menges, M. Kastler, M. Baumgarten and K. Müllen, *ChemSusChem*, 2010, **3**, 106.
14 S. Xiao, H. Zhou and W. You, *Macromolecules*, 2008, **41**, 5688.
15 M. Yuan, A. H. Rice and C. K. Luscombe, *J. Polym. Sci., Part A: Polym. Chem.*, 2011, **49**, 701.
16 S. Xiao, A. C. Stuart, S. Liu and W. You, *ACS Appl. Mater. Interfaces*, 2009, **1**, 1613.
17 H. Zhou, L. Yang, S. Stoneking and W. You, *ACS Appl. Mater. Interfaces*, 2010, **2**, 1377.
18 H. Zhou, L. Yang, S. C. Price, K. J. Knight and W. You, *Angew. Chem., Int. Ed.*, 2010, **49**, 7992.
19 L. Yang, J. R. Tumbleston, H. Zhou, H. Ade and W. You, *Energy Environ. Sci.*, 2013, **6**, 316.
20 R. Rieger, D. Beckmann, W. Pisula, W. Steffen, M. Kastler and K. Müllen, *Adv. Mater.*, 2010, **22**, 83.
21 R. Rieger, D. Beckmann, A. Mavrinskiy, M. Kastler and K. Müllen, *Chem. Mater.*, 2010, **22**, 5314.
22 Y. Didane, G. H. Mehl, A. Kumagai, N. Yoshimoto, C. Videlot-Ackermann and H. Brisset, *J. Am. Chem. Soc.*, 2008, **130**, 17681.
23 R. Fitzner, E. Reinold, A. Mishra, E. Mena-Osteritz, H. Ziehlke, C. Körner, K. Leo, M. Riede, M. Weil, O. Tsaryova, A. Weiß, C. Uhrich, M. Pfeiffer and P. Bäuerle, *Adv. Funct. Mater.*, 2011, **21**, 897.
24 T. Qi, Y. Liu, W. Qiu, H. Zhang, X. Gao, Y. Liu, K. Lu, C. Du, G. Yu and D. Zhu, *J. Mater. Chem.*, 2008, **18**, 1131.
25 R. Fitzner, C. Elschner, M. Weil, C. Uhrich, C. Körner, M. Riede, K. Leo, M. Pfeiffer, E. Reinold, E. Mena-Osteritz and P. Bäuerle, *Adv. Mater.*, 2012, **24**, 675.
26 G. S. Grubb, P. Zhang, E. A. Terefenko, A. Fensome, J. E. Wrobel, H. Fletcher III, J. P. Edwards, T. K. Jones, C. M. Tegley, L. Zhi, *US Pat.*, 0045511, 2003.
27 S. Yoshida, M. Fujii, Y. Aso, T. Otsubo and F. Ogura, *J. Org. Chem.*, 1994, **59**, 3077.
28 Y. A. Getmanenko, P. Tongwa, T. V. Timofeeva and S. R. Marder, *Org. Lett.*, 2010, **12**, 2136.
29 J. Verron, P. Malherbe, E. Prinssen, A. W. Thomas, N. Nock and R. Masciadri, *Tetrahedron Lett.*, 2007, **48**, 377.
30 J. A. Letizia, S. Cronin, R. P. Ortiz, A. Facchetti, M. A. Ratner and T. J. Marks, *Chem.–Eur. J.*, 2010, **16**, 1911.

31 J. D. Tovar, A. Rose and T. M. Swager, *J. Am. Chem. Soc.*, 2002, **124**, 7762.
32 K. E. S. Phillips, T. J. Katz, S. Jockusch, A. J. Lovinger and N. J. Turro, *J. Am. Chem. Soc.*, 2001, **123**, 11899.
33 J. D. Tovar and T. M. Swager, *Adv. Mater.*, 2001, **13**, 1775.
34 O. Gidron, Y. Diskin-Posner and M. Bendikov, *J. Am. Chem. Soc.*, 2010, **132**, 2148.
35 T. Johansson, W. Mammo, M. Svensson, M. R. Andersson and O. Inganäs, *J. Mater. Chem.*, 2003, **13**, 1316.
36 Q. Xie, F. Arias and L. Echegoyen, *J. Am. Chem. Soc.*, 1993, **115**, 9818.
37 M. Riede, T. Müller, W. Tress, R. Schüppel and K. Leo, *Nanotechnology*, 2008, **19**, 424001.
38 J. Drechsel, B. Maennig, D. Gebeyehu, M. Pfeiffer, K. Leo and H. Hoppe, *Org. Electron.*, 2003, **5**, 175.
39 D. Wynands, M. Levichkova, M. Riede, M. Pfeiffer, P. Bäuerle, R. Rentenberger, P. Denner and K. Leo, *J. Appl. Phys.*, 2010, **107**, 014517.
40 C. Uhrich, D. Wynands, S. Olthof, M. Riede, K. Leo, S. Sonntag, B. Maennig and M. Pfeiffer, *J. Appl. Phys.*, 2008, **4**, 43107.
41 A. Cravino, P. Leriche, O. Alévêque, S. Roquet and J. Roncali, *Adv. Mater.*, 2006, **18**, 3033.
42 S. Steinberger, A. Mishra, E. Reinold, C. M. Müller, C. Uhrich, M. Pfeiffer and P. Bäuerle, *Org. Lett.*, 2011, **13**, 90.
43 H. J. Snaith, N. C. Greenham and R. H. Friend, *Adv. Mater.*, 2004, **16**, 1640.
44 C. Uhrich, R. Schueppel, A. Petrich, M. Pfeiffer, K. Leo, E. Brier, P. Kilickiran and P. Bäuerle, *Adv. Funct. Mater.*, 2007, **17**, 2991.
45 S. Haid, A. Mishra, C. Uhrich, M. Pfeiffer and P. Bäuerle, *Chem. Mater.*, 2011, **23**, 4435.
46 D. Wynands, M. Levichkova, K. Leo, C. Uhrich, G. Schwartz, D. Hildebrandt, M. Pfeiffer and M. Riede, *Appl. Phys. Lett.*, 2010, **97**, 073503.
47 M. W. Andersen, B. Hildebrandt, G. Köster and R. W. Hoffmann, *Chem. Ber.*, 1989, **122**, 1777.
48 R. Rieger, Extended Donor and Acceptor Molecules for Organic Electronics, dissertation, Johannes Gutenberg-Universität (Mainz), 2009.
49 W. J. Kerr, A. J. Morrison, M. Pazicky and T. Weber, *Org. Lett.*, 2012, **14**, 2250–2253.
50 F. A. Arroyave, C. A. Richard and J. R. Reynolds, *Org. Lett.*, 2012, **14**, 6138–6141.
51 B. Rungtaweevoranit, A. Butsuri, K. Wongma, K. Sadorn, K. Neranon, C. Nerungsi and T. Thongpanchang, *Tetrahedron Lett.*, 2012, **53**, 1816.